

Floquet Topological Magnons

S. A. Owerre¹

¹*Perimeter Institute for Theoretical Physics, 31 Caroline St. N., Waterloo, Ontario N2L 2Y5, Canada.*

We introduce the concept of Floquet topological magnons — a mechanism by which a synthetic tunable Dzyaloshinskii-Moriya interaction (DMI) can be generated in quantum magnets using circularly polarized electric (laser) field. The resulting effect is that Dirac magnons and nodal-line magnons in two-dimensional (2D) and three-dimensional (3D) quantum magnets can be tuned to magnon Chern insulators and Weyl magnons respectively under circularly polarized laser field. The Floquet formalism also yields a tunable intrinsic DMI in insulating quantum magnets without an inversion center. We demonstrate that the Floquet topological magnons possess a finite thermal Hall conductivity tunable by the laser field.

Quantum magnets without an inversion center allow an intrinsic Dzyaloshinskii-Moriya interaction (DMI) [1, 2], which is a consequence of spin-orbit coupling (SOC) and it is usually fixed in different magnets. The associated magnon bands in the magnetically ordered systems have a nontrivial topology with Chern number protected chiral magnon edge modes in 2D systems and magnon surface states in 3D systems. They are dubbed topological magnon Chern insulators [3–9] and Weyl magnons [10–13] respectively. They are the analogs of electronic topological (Chern) insulators [14–16] and Weyl semimetals [17–19]. However, due to the charge-neutral property of magnons, topological magnonic materials are believed to be potential candidates for low-dissipation magnon transports in insulating quantum magnets and they are applicable to magnon spintronics and magnetic data storage [20]. Topological magnonic materials (*i.e.* magnon Chern insulators and Weyl magnons) also possess a thermal Hall effect as predicted theoretically [21–25] and observed experimentally [26–28]. To date, topological magnon bands have been realized only in a quasi-2D kagomé ferromagnet [29].

Generally, every quantum ferromagnetic material does not have a strong intrinsic DMI necessary for topological magnons to exist. For instance, the single crystals of the ferromagnetic honeycomb compounds CrX_3 ($\text{X} \equiv \text{Br}, \text{Cl}, \text{and I}$) show no evidence of DMI [30–35], and kagomé haydeeite also does not have a finite (topological) energy gap in the observed spin-wave spectra [36], suggesting that the DMI does not play a significant role in haydeeite. These 2D ferromagnetic materials with negligible DMI are candidates for Dirac magnons [37], and the 3D ferromagnetic counterparts are candidates for nodal-line magnons [13, 38]. By applying a circularly polarized laser field in these “topologically trivial” systems, one can generate topological magnons (*i.e.*, magnon Chern insulators and Weyl magnons) via a tunable synthetic laser-induced DMI. This is particularly important as it offers a way to tune the DMI in magnetic materials.

The Floquet theory [39] of laser-driven systems provides a theoretical as well as experimental method to engineer such topologically nontrivial systems. This formalism is mostly dominated by electronic systems [40–59] and also optical bosonic systems [60–65]. Moreover, an

applied laser field provides a means for coherent control of the magnetization in 1D quantum magnets [66–70].

In this Letter, we introduce the Floquet formalism to 2D and 3D ferromagnetic quantum magnets in the presence of a circularly polarized electric (laser) field. We show that the underlying charge-neutral magnons acquire a time-dependent Aharonov-Casher phase [71], which generates a tunable synthetic DMI in magnetic systems with negligible intrinsic DMI. This leads to emergent nontrivial magnon Chern insulators and Weyl magnons with finite thermal Hall conductivity, which can be manipulated by the laser field. Our results provide a novel platform to engineer topological magnons in topologically trivial insulating quantum magnets. We hope that these results will extend the experimental search for topological magnons to a broader class of insulating quantum magnetic materials even without an intrinsic DMI.

Let us consider 2D and 3D ferromagnetic spin systems described by the pristine Hamiltonian

$$\mathcal{H}_0 = -J \sum_{\langle \alpha, \beta \rangle} \mathbf{S}_\alpha \cdot \mathbf{S}_\beta, \quad (1)$$

where $\langle \alpha, \beta \rangle$ denotes summation over nearest-neighbour (NN) sites and \mathbf{S}_α are the magnetic spin vectors at the lattice sites α located at \mathbf{r}_α and J is the ferromagnetic interaction. For now we take the intrinsic DMI to be negligible, which is the case in most ferromagnetic compounds. Therefore, the goal is to generate a synthetic DMI by periodic modulation of the lattice using a time-dependent electric field of a laser light.

We are interested in the underlying magnon excitations of the quantum spin Hamiltonian (1) as described by the Holstein-Primakoff transformation: $S_\alpha^z = S - a_\alpha^\dagger a_\alpha$, $S_\alpha^+ \approx \sqrt{2S} a_\alpha = (S_\alpha^-)^\dagger$, where $a_\alpha^\dagger (a_\alpha)$ are the bosonic creation (annihilation) operators, and $S_\alpha^\pm = S_\alpha^x \pm iS_\alpha^y$ denote the spin creation and annihilation operators which correspond to the hopping terms. However, we will retain the spin operators in order to show the explicit form of the laser-induced DMI. As magnons are charge-neutral bosonic quasi-particles they do not interact with electromagnetic field except through their magnetic dipole moment, which we assume to be in the z -direction $\boldsymbol{\mu} = g\mu_B \hat{\mathbf{z}}$, where μ_B is the Bohr magneton and g the Landé g -factor. Now suppose that a circularly po-

larized laser (electromagnetic) field with dominant oscillating electric field components $\mathbf{E}(t)$ is irradiated perpendicular to the magnetic material lying on the x - y plane. The magnetic dipole moment of magnon quasi-particles hopping in such an electric field background will acquire the time-dependent Aharonov-Casher phase [71]

$$\theta_{\alpha\beta}(t) = \frac{g\mu_B}{\hbar c^2} \int_{\mathbf{r}_\alpha}^{\mathbf{r}_\beta} (\mathbf{E}(t) \times \hat{z}) \cdot d\ell, \quad (2)$$

where \hbar is the reduced Planck's constant and c is the speed of light. The oscillating electric field obeys the relation $\mathbf{E}(t) = -\partial \mathbf{A}(t)/\partial t$, where $\mathbf{A}(t)$ is the time-periodic vector potential. We choose an oscillating electric field such that

$$\mathbf{E}(t) \times \hat{z} = E_0(\sin \omega t, -\cos \omega t, 0), \quad (3)$$

where E_0 is the amplitude of the electric field. The corresponding time-dependent Hamiltonian is given by

$$\mathcal{H}(t) = - \sum_{\langle \alpha, \beta \rangle} \left[\frac{J}{2} \left(S_\alpha^- S_\beta^+ e^{i\theta_{\alpha\beta}(t)} + h.c. \right) + JS_\alpha^z S_\beta^z \right], \quad (4)$$

Noticing that the direction of the vector pointing from \mathbf{r}_α to \mathbf{r}_β defines a relative angle $\phi_{\alpha\beta}$, we get $\theta_{\alpha\beta}(t) = \lambda \sin(\omega t - \phi_{\alpha\beta})$ where

$$\lambda = \frac{g\mu_B E_0 a}{\hbar c^2}, \quad (5)$$

is the dimensionless parameter characterizing the light intensity in the magnonic Floquet formalism and a is the lattice constant. Notice the difference between the dimensionless parameter in Eq. (5) and that of electronic Floquet formalism [41, 43].

The Floquet theory is a standard mechanism to study driven quantum systems in the likes of Eq. 4 [40–43]. It enables one to transform a time-dependent model into a static effective model governed by what is called the Floquet Hamiltonian. Now, we proceed with this formalism. The static time-independent effective Hamiltonian can be expanded in the power series of ω^{-1} and it is given by $\mathcal{H}_{\text{eff}} = \sum_{i \geq 0} \omega^{-i} \mathcal{H}_{\text{eff}}^{(i)}$. We calculate the series expansion of the effective Hamiltonian using the discrete Fourier component of the time-dependent Hamiltonian $\mathcal{H}^n = \frac{1}{T} \int_0^T dt e^{-in\omega t} \mathcal{H}(t)$ with period $T = 2\pi/\omega$, where

$$\mathcal{H}^n = - \sum_{\langle \alpha, \beta \rangle} \left[\frac{J_{n,\perp}}{2} \left(S_\alpha^- S_\beta^+ e^{-in\phi_{\alpha\beta}} + h.c. \right) + J\delta_{n,0} S_\alpha^z S_\beta^z \right], \quad (6)$$

with $J_{n,\perp} = J\mathcal{J}_n(\lambda)$, and $\mathcal{J}_n(\lambda)$ is the Bessel function of order $n \in \mathbb{Z}$. $\delta_{n,\ell} = 1$ for $n = \ell$ and zero otherwise. We have used the standard relation $e^{[iz \sin(x)]} = \sum_{m=-\infty}^{\infty} \mathcal{J}_m(z) e^{imx}$. In the high frequency limit $\omega \gg J$

the leading order contribution is the zeroth order effective Hamiltonian given by $\mathcal{H}_{\text{eff}}^{(0)} = \mathcal{H}^0$, where

$$\mathcal{H}_{\text{eff}}^{(0)} = - \sum_{\langle \alpha, \beta \rangle} [J_{0,\perp} (S_\alpha^x S_\beta^x + S_\alpha^y S_\beta^y) + JS_\alpha^z S_\beta^z], \quad (7)$$

and $J_{0,\perp} = J\mathcal{J}_0(\lambda)$. Thus, the zeroth order term yields an XXZ ferromagnetic Hamiltonian. For quantum spin-1/2 ferromagnetic systems, Eq. 7 is equivalent to the Bose-Einstein condensation of hardcore bosons studied by Matsubara and Matsuda [72], but in this case $J \geq |J_{0,\perp}|$. By lowering the frequency the first order contribution to the effective Hamiltonian is non-negligible. It is given by

$$\mathcal{H}_{\text{eff}}^{(1)} = \sum_{n=1}^{\infty} \frac{1}{n} [\mathcal{H}^n, \mathcal{H}^{-n}]. \quad (8)$$

The commutator of the spin operators results in a product of three spins reminiscent of the scalar spin chirality. In order to see this we note that the z -component of the spins vanishes for $n \geq 1$, therefore the commutation relation in the first order term involves only $[S_\alpha^+ S_\beta^-, S_\rho^+ S_\gamma^-] = 2(\delta_{\beta\rho} S_\beta^z S_\alpha^+ S_\gamma^- - \delta_{\alpha\gamma} S_\alpha^z S_\rho^+ S_\beta^-)$. We use this relation together with the identity $\mathcal{J}_{-n}(z) = (-)^n \mathcal{J}_n(z)$ and obtain

$$\mathcal{H}_{\text{eff}}^{(1)} = \sum_{\Delta/\nabla} J_{\alpha\beta}^{(1)} \mathbf{S}_\gamma \cdot (\mathbf{S}_\alpha \times \mathbf{S}_\beta), \quad (9)$$

where

$$J_{\alpha\beta}^{(1)} = - \sum_{n=1}^{\infty} 2(-)^n J_{n,\perp}^2 \sin(n\Phi_{\alpha\beta}), \quad (10)$$

with $\Phi_{\alpha\beta} = \phi_{\alpha\gamma} - \phi_{\beta\gamma}$. $\mathbf{S}_\gamma = S_\gamma^z \hat{z}$ and γ is the intermediate lattice site between α and β [21] and the sum is over the triangular plaquettes of the chosen lattice geometry.

The main result of this Letter is the induced synthetic DMI by circularly polarized laser field as given in Eq. (9). The DMI points along the z -direction perpendicular to the x - y plane. On the kagomé and pyrochlore lattices the synthetic DMI lies within the bonds of the NN sites, whereas on the honeycomb lattice it lies within the bonds of the next-nearest neighbour (NNN) sites. The DMI is the primary source of magnon Chern insulators and Weyl magnons in insulating quantum ferromagnets. Consequently, Dirac magnons in 2D ferromagnetic systems and nodal-line magnons in 3D ferromagnetic systems with negligible intrinsic DMI will be driven to magnon Chern insulators and Weyl magnons respectively by the circularly polarized laser field.

Now, we exemplify this method by utilizing the 2D honeycomb ferromagnets for simplicity (see Fig. 1). In this case the relative angle is given by $\phi_{\alpha\gamma} - \phi_{\beta\gamma} = \frac{2\pi}{3} \nu_{\alpha\beta}$ [57, 58], where $\nu_{\alpha\beta} = +/-$ for hopping within Δ/∇ respectively. Hence $J_{\alpha\beta}^{(1)} \approx \sqrt{3} \nu_{\alpha\beta} J_{1,\perp}^2$. The total effective

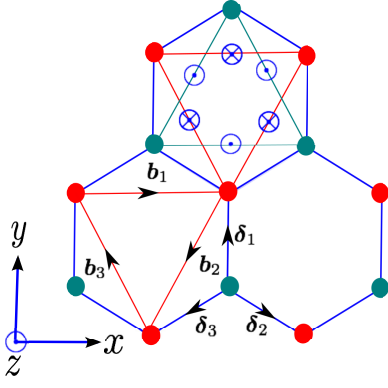


FIG. 1. The schematic of the honeycomb lattice with laser-field-induced DMI. The blue dotted and crossed circles denote the direction of the synthetic DM vectors pointing in and out of the lattice plane on the NNN bonds. Here, δ_i are the vectors connecting the NN sites and \mathbf{b}_i connect the NNN sites. The different colours of the solid circles red(green) are used to denote the two sublattices $A(B)$.

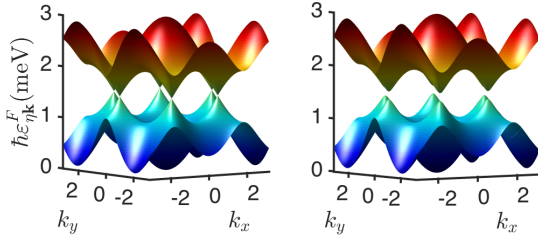


FIG. 2. Floquet magnon band structure of circularly laser-driven honeycomb quantum ferromagnetic spin system for $J = 1$ meV $\lambda = 1.5$ in units of $g\mu_B a/\hbar c^2$ and $\hbar\omega = 2.5$. (i) Floquet Dirac magnon in the zeroth order approximation $D_F = 0$. (ii) Floquet topological magnon in the first order approximation $D_F \simeq 0.014J$.

Floquet Hamiltonian up to first order is given by

$$\mathcal{H}_{\text{eff}} = - \sum_{\langle \alpha\beta \rangle} [J_{0,\perp}(S_\alpha^x S_\beta^x + S_\alpha^y S_\beta^y) + JS_\alpha^z S_\beta^z] \quad (11)$$

$$+ D_F \sum_{\Delta/\nabla} \nu_{\alpha\beta} \mathbf{S}_\gamma \cdot (\mathbf{S}_\alpha \times \mathbf{S}_\beta),$$

where $D_F = \sqrt{3}J_{1,\perp}^2/\omega$. We note that $|J_{0,\perp}| \leq J$, so that the spins would prefer to order magnetically along the z -direction. The synthetic DMI does not affect the ferromagnetic ordering of the spins. We study the underlying magnon excitations of Eq. 11 by implementing the linear order Holstein-Primakoff transformation mentioned above on the two sublattices A and B of the honeycomb lattice. In the bosonic representation the synthetic DMI is imaginary. It generates a synthetic magnetic gauge flux within the NNN sites. The momentum space Hamiltonian is given by

$$\mathcal{H}_{\text{eff}}(\mathbf{k}) = h_0 \mathbf{I}_{2 \times 2} + \mathbf{h}(\mathbf{k}) \cdot \boldsymbol{\sigma}, \quad (12)$$

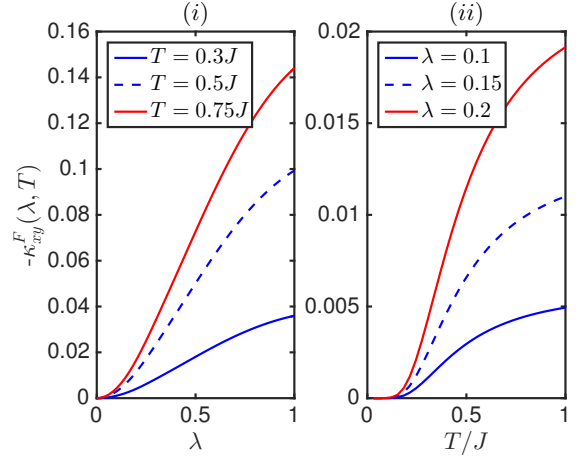


FIG. 3. Floquet tunable thermal Hall conductivity. (i) κ_{xy}^F vs. λ for different temperatures. (ii) κ_{xy}^F vs. T for different amplitudes. Here, $J = 1$ meV and $\hbar\omega = 2.5J$.

where $\boldsymbol{\sigma} = (\sigma_x, \sigma_y, \sigma_z)$ are Pauli matrices and $\mathbf{I}_{2 \times 2}$ is an identity 2×2 matrix. $h_0 = 3JS$, and $\mathbf{h}(\mathbf{k}) = (h_x(\mathbf{k}), h_y(\mathbf{k}), h_z(\mathbf{k}))$, with $h_x(\mathbf{k}) = -J_{0,\perp} S \sum_j \cos \mathbf{k} \cdot \boldsymbol{\delta}_j$, $h_y(\mathbf{k}) = -J_{0,\perp} S \sum_j \sin \mathbf{k} \cdot \boldsymbol{\delta}_j$, and $h_z(\mathbf{k}) = 2D_F S^2 \sum_j \sin \mathbf{k} \cdot \mathbf{b}_j$. The Floquet magnon bands are given by

$$\varepsilon_{\eta\mathbf{k}}^F = h_0 + \eta \sqrt{\mathbf{h}(\mathbf{k}) \cdot \mathbf{h}(\mathbf{k})}, \quad (13)$$

where $\eta = \pm$ labels the top and the bottom bands respectively. Henceforth we set $S = 1/2$. The Floquet magnon bands are depicted in Fig. 2 for zeroth order (i) and first order (ii) contributions to the effective Hamiltonian. In the former (i), the system exhibits Dirac magnon points in the undriven systems [37] because the Floquet Dirac magnons can be manipulated by anisotropic laser field amplitude, *i.e.*, $A_0 = (A_x, A_y, 0)$. In this case the Dirac magnon points can move away from the high symmetry points of the Brillouin zone at $\pm \mathbf{K} = (\pm 4\pi/3\sqrt{3}, 0)$ and can also be gapped out by fine-tuning the anisotropic amplitudes. However, the system will still remain topologically trivial at the zeroth order as time-reversal symmetry is preserved.

A nontrivial band topology arises by lowering the frequency and the first order correction becomes important, which breaks time-reversal symmetry. This leads to a synthetic DMI which induces a gap ($\Delta_{\text{gap}} \sim 2|D_F|$) at the Dirac points as shown in Fig. 2(ii). The Floquet magnon bands now acquire a nonzero Berry curvature which has the form $\Omega_{\eta\mathbf{k}}^F = (\nabla \times \mathcal{A}_{\eta\mathbf{k}}^F)_z$ where $\mathcal{A}_{\eta\mathbf{k}}^F = i \langle \psi_{\eta\mathbf{k}}^F | \nabla | \psi_{\eta\mathbf{k}}^F \rangle$ is the Berry connection and $\psi_{\eta\mathbf{k}}^F$ are the Floquet eigenvectors of $\mathcal{H}_{\text{eff}}(\mathbf{k})$. The Floquet Chern numbers are given by the integration of the Berry curvatures over the Brillouin zone,

$$C_\eta^F = \frac{1}{2\pi} \int_{BZ} d^2k \Omega_{\eta\mathbf{k}}^F. \quad (14)$$

It is easily shown that the Floquet Chern numbers are proportional to the synthetic DMI: $\mathcal{C}_\eta^F \sim \eta \text{sgn}[D_F]$, which can be controlled by the laser field.

The nontrivial topology of the Floquet magnon bands has an important transport consequences. It can lead to Floquet thermal magnon Hall effect. This refers to the generation of a transverse heat current upon the application of a longitudinal temperature gradient. In this case, the synthetic laser-field-induced Berry curvature due to the DMI appear in the equations of motion of a magnon wave packet in the same mathematical structure as a magnetic field in the Lorentz force. In other words, the Berry curvature due to the DMI acts like an effective magnetic field in momentum space on the magnons. The resulting effect is the production of a transverse thermal Hall conductivity, which can derived from linear response theory [22]. The Floquet thermal Hall conductivity is given by

$$\kappa_{xy}^F(\lambda, T) = -\frac{k_B^2 T}{(2\pi)^2 \hbar} \sum_{\eta=\pm} \int_{BZ} d^2 k c_2(n_\eta) \Omega_{\eta\mathbf{k}}^F, \quad (15)$$

where $n_\eta \equiv n_B(\varepsilon_{\eta\mathbf{k}}) = (e^{\varepsilon_{\eta\mathbf{k}}/k_B T} - 1)^{-1}$ is the Bose function close to thermal equilibrium, $c_2(x) = (1+x)(\ln \frac{1+x}{x})^2 - (\ln x)^2 - 2\text{Li}_2(-x)$, and $\text{Li}_n(x)$ is a polylogarithm. In Fig. 3 we have shown the plots of $\kappa_{xy}^F(\lambda, T)$ as functions of the parameters in units of k_B/\hbar . For the two-band honeycomb ferromagnets the Floquet thermal Hall conductivity is negative and it is tunable by the amplitude (frequency) of the laser field. In particular, $\kappa_{xy}^F(\lambda, T)$ can be tuned off at the zeros of $\mathcal{J}_n(\lambda)$. This is usually not possible in materials with a strong intrinsic DMI in the absence of a laser field.

However, applying circularly polarized laser field in magnetic materials with a strong intrinsic DMI can induce a tunable DMI. Using the simple honeycomb ferromagnetic model as an example, the suitable DMI due to inversion symmetry breaking of the lattice is of the form [7] $\mathcal{H}_{DMI} = D_0 \sum_{\langle\langle\alpha\beta\rangle\rangle} \nu_{\alpha\beta} \hat{\mathbf{z}} \cdot \mathbf{S}_\alpha \times \mathbf{S}_\beta$, where the summation is taken over the triangular plaquettes of the NNN sites. In the presence of a circularly polarized laser field with sufficiently high frequency, the zeroth order correction to the effective Hamiltonian gives $\mathcal{H}_{DMI}^{\text{eff}} = D_0 \mathcal{J}_0(\lambda) \sum_{\langle\langle\alpha\beta\rangle\rangle} \nu_{\alpha\beta} \hat{\mathbf{z}} \cdot \mathbf{S}_\alpha \times \mathbf{S}_\beta$. Now the value of the intrinsic DMI can be manipulated by varying λ . For $\lambda < \lambda_c \approx 2.4048$ a gap exists at the Dirac points and it closes near the first zero of the Bessel function $\lambda \approx \lambda_c$ and reopens for $\lambda > \lambda_c$. Consequently, the sign of the Chern numbers (Berry curvatures) of the two bands changes as shown in Fig. 4. Hence, a sign change emerges in $\kappa_{xy}^F(\lambda, T)$ (not shown). We note that a sign change is not possible in the undriven system on the honeycomb lattice [8, 9]. The complete topological phase transition including a trivial insulating regime with zero Chern number can be found by including NNN Heisenberg interaction as we have shown in the supplemental material [73].

It is important to note that the circularly polarized

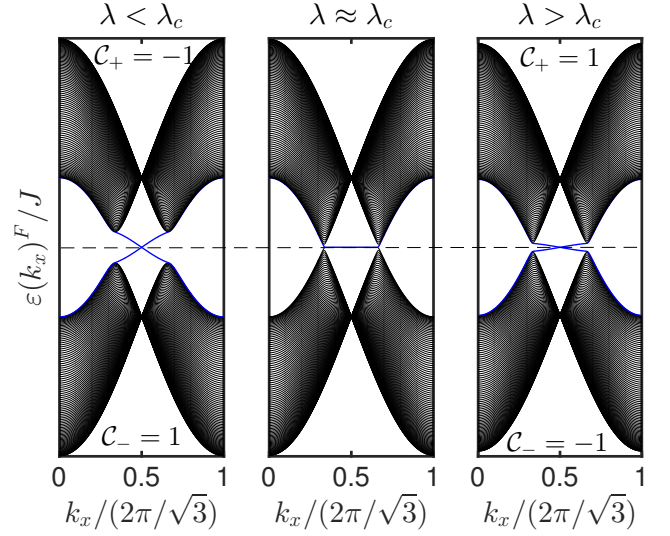


FIG. 4. Evolution of sign change in the Floquet Chern numbers of honeycomb ferromagnets with tunable intrinsic DMI for different values of λ in units of $g\mu_B a/\hbar c^2$ and $D_0/J = 0.15$. The black lines are the magnon bulk bands and blue lines denote the chiral magnon edge modes gapless at $\varepsilon(k_x = \pi/\sqrt{3}) = h_0$ as indicated by the dashed line.

laser field is necessary to induce a tunable synthetic DMI in quantum ferromagnets with negligible intrinsic DMI. However, in frustrated magnets with a coplanar magnetic order, a static magnetic field applied perpendicular to the plane of the magnets can induce a tunable synthetic scalar spin chirality due to non-coplanar spin configurations. In this case tunable topological magnons can be produced even in the absence of an intrinsic DMI [74–76].

In conclusion, we have shown that the time-dependent Aharonov-Casher phase acquired by charge-neutral magnons in a time varying circularly polarized electric (laser) field induces a synthetic DMI, leading to non-trivial topological magnons in the absence of an intrinsic DMI. Therefore, Dirac magnons and nodal-line magnons become magnon Chern insulators and Weyl magnons respectively under radiation. Our results also showed that the intrinsic DMI in insulating quantum magnets without an inversion symmetry can be manipulated with circularly polarized laser field. Hence, the emergent thermal Hall effect can be turned. It is experimentally feasible to investigate the proposed phenomena in magnetic insulators using ultrafast terahertz spectroscopy [77]. This formalism may find application in the switching of magnetization and magnon spin current by a laser field as an important step towards magnon spintronics and magnetic data storage [78, 79]. We believe that these results will extend the study of topological magnons to different magnetic materials without any restrictions. In an inhomogeneous static electric field a time-independent Aharonov-Casher phase can be acquired by magnons and leads to magnonic Landau levels in insulating magnets [80].

Research at Perimeter Institute is supported by the Government of Canada through Industry Canada and by

the Province of Ontario through the Ministry of Research and Innovation.

-
- [1] I. Dzyaloshinsky, J. Phys. Chem. Solids **4**, 241 (1958).
 - [2] T. Moriya, Phys. Rev. **120**, 91 (1960).
 - [3] L. Zhang, J. Ren, J. -S. Wang, and B. Li, Phys. Rev. B **87**, 144101 (2013).
 - [4] R. Shindou et.al., Phys. Rev. B **87**, 174427 (2013); Phys. Rev. B **87**, 174402 (2013).
 - [5] A. Mook, J. Henk and I. Mertig, Phys. Rev. B. **90**, 024412 (2014). Phys. Rev. B. **89**, 134409 (2014).
 - [6] X. Cao, K. Chen and D. He, J. Phys.: Condens. Matter **27**, 166003 (2015).
 - [7] S. A. Owerre, J. Phys.: Condens. Matter **28**, 386001 (2016).
 - [8] S. A. Owerre, J. Appl. Phys. **120**, 043903 (2016).
 - [9] S. K. Kim et.al., Y. Tserkovnyak, Phys. Rev. Lett. **117**, 227201 (2016).
 - [10] F. -Y. Li et.al., Nat. Commun. **7**, 12691 (2016).
 - [11] A. Mook, J. Henk, and I. Mertig, Phys. Rev. Lett. **117**, 157204 (2016).
 - [12] S. Ying, X. S. Wang, and X. R. Wang, Phys. Rev. B **95**, 224403 (2017).
 - [13] K. Li and J. Hu, Chin. Phys. Lett. **34**, 077501 (2017).
 - [14] X.-L. Qi and S.-C. Zhang, Rev. Mod. Phys. **83**, 1057 (2011).
 - [15] M. Z. Hasan and C. L. Kane, Rev. Mod. Phys. **82**, 3045 (2010).
 - [16] F. D. M. Haldane, Phys. Rev. Lett. **61**, 2015 (1988).
 - [17] X. Wan et.al., Phys. Rev. B **83**, 205101 (2011).
 - [18] L. Balents, Physics **4**, 36 (2011).
 - [19] A. A. Burkov and L. Balents, Phys. Rev. Lett. **107**, 127205 (2011).
 - [20] A. V. Chumak, V. I. Vasyuchka, A. A. Serga, and B. Hillebrands, Nature Phys. **11**, 453 (2015).
 - [21] H. Katsura, N. Nagaosa, and P. A. Lee, Phys. Rev. Lett. **104**, 066403 (2010).
 - [22] R. Matsumoto and S. Murakami, Phys. Rev. Lett. **106**, 197202 (2011).
 - [23] R. Matsumoto and S. Murakami, Phys. Rev. B. **84**, 184406 (2011).
 - [24] H. Lee, J. H. Han, and P. A. Lee, Phys. Rev. B. **91**, 125413 (2015).
 - [25] R. Matsumoto, R. Shindou, and S. Murakami, Phys. Rev. B **89**, 054420 (2014).
 - [26] Y. Onose et.al., Science **329**, 297 (2010).
 - [27] T. Ideue et.al., Phys. Rev. B. **85**, 134411 (2012).
 - [28] M. Hirschberger et.al., Phys. Rev. Lett. **115**, 106603 (2015).
 - [29] R. Chisnell et.al., Phys. Rev. Lett. **115**, 147201 (2015).
 - [30] A. C. Gossard, V. Jaccarino, and J. P. Remeika, Phys. Rev. Lett. **7**, 122 (1961)
 - [31] H. L. Davis and A. Narath, Phys. Rev. **134**, A433 (1964).
 - [32] E. J. Samuelsen et.al., Phys. Rev. B **3**, 157 (1971).
 - [33] A. Narath and H. L. Davis, Phys. Rev. **137**, A163 (1965).
 - [34] B. Huang, et al., Nature **546**, 270 (2017).
 - [35] J. L. Lado and J. F. -Rossier, 2D Mater. **4**, 035002 (2017).
 - [36] D. Boldrin et.al., Phys. Rev. B **91**, 220408(R) (2015).
 - [37] J. Fransson, A. M. Black-Schaffer, and A. V. Balatsky, Phys. Rev. B **94**, 075401 (2016).
 - [38] A. Mook, J. Henk, I. Mertig, Phys. Rev. B **95**, 014418 (2017).
 - [39] J. H. Shirley, Phys. Rev. **138**, B979 (1965).
 - [40] T. Oka, and H. Aoki, Phys. Rev. B **79**, 081406 (2009).
 - [41] J. -i. Inoue and A. Tanaka, Phys. Rev. Lett. **105**, 017401 (2010).
 - [42] H. L. Calvo et.al., Appl. Phys. Lett. **98**, 232103 (2011).
 - [43] T. Kitagawa et al., Phys. Rev. B **84**, 235108 (2011).
 - [44] J. Cayssol et.al., Physica Status Solidi (RRL)-Rapid Research Letters **7**, 101 (2013).
 - [45] P. Delplace, Á. Gómez-León, and Gloria Platero, Phys. Rev. B **88**, 245422 (2013)
 - [46] A. G. Grushin, Á. Gómez-León, and T. Neupert, Phys. Rev. Lett. **112**, 156801 (2014).
 - [47] G. Jotzu et al. Nature **515**, 237 (2014).
 - [48] N. Fläschner, et al. Science **352**, 1091 (2016).
 - [49] R. Wang et.al., EPL (Europhys. Lett.) **105**, 17004 (2014).
 - [50] S. Ebihara, K. Fukushima, and T. Oka, Phys. Rev. B **93**, 155107 (2016).
 - [51] C.-K. Chan et.al., Phys. Rev. Lett. **116**, 026805 (2016).
 - [52] Z. Yan and Z. Wang, Phys. Rev. Lett. **117**, 087402 (2016).
 - [53] X.-X. Zhang, T. Tzen Ong, and N. Nagaosa, Phys. Rev. B **94**, 235137 (2016).
 - [54] H. Hübener et.al., Nat. Comm. **8**, 13940 (2017).
 - [55] N. Goldman and J. Dalibard, Phys. Rev. X **4**, 031027 (2014).
 - [56] M. Bukov, L. D'Alessio, and A. Polkovnikov, Advances in Physics **64**, 139, (2015).
 - [57] A. Eckardt and E. Anisimovas, New J. Phys. **17**, 093039 (2015).
 - [58] A. Eckardt, Rev. Mod. Phys. **89**, 011004 (2017).
 - [59] E. A. Stepanov, C. Dutreix, and M. I. Katsnelson, Phys. Rev. Lett. **118**, 157201 (2017).
 - [60] A. Eckardt, C. Weiss, and M. Holthaus, Phys. Rev. Lett. **95**, 260404 (2005).
 - [61] J. Struck, et al. Science **333**, 996 (2011).
 - [62] J. Struck, et al. Phys. Rev. Lett. **108**, 225304 (2012).
 - [63] J. Struck, et al. Nat. Phys. **9**, 738 (2013).
 - [64] C. J. Kennedy, et al. Nat. Phys. **11**, 859 (2015).
 - [65] K. Plekhanov, G. Roux, and K. Le Hur, Phys. Rev. B **95**, 045102 (2017).
 - [66] S. Takayoshi, H. Aoki, and T. Oka, Phys. Rev. B **90**, 085150 (2014).
 - [67] S. Takayoshi, M. Sato, T. Oka, Phys. Rev. B **90**, 214413 (2014).
 - [68] A. A. Zvyagin, Phys. Rev. B **92**, 054405 (2015).
 - [69] M. Sato, S. Takayoshi, and T. Oka, Phys. Rev. Lett. **117**, 147202 (2016).
 - [70] J. Herbrich, X. Zotos, Phys. Rev. B **93**, 134412 (2016).
 - [71] Y. Aharonov and A. Casher, Phys. Rev. Lett. **53**, 319 (1984).
 - [72] T. Matsubara and H. Matsuda, Prog. Theor. Phys. **16**, 569 (1956).
 - [73] See the Supplemental Material.
 - [74] S. A. Owerre, Phys. Rev. B **95**, 014422 (2017).

- [75] S. A. Owerre, J. Phys.: Condens. Matter **29**, 03LT01 (2017).
- [76] S. A. Owerre, EPL (Europhys. Lett.) **117**, 37006 (2017).
- [77] E. Baldini, Private Communication.
- [78] X. Zhang et.al., Phys. Rev. Lett. **113**, 037202 (2014).
- [79] A. J. Schellekens et.al., Nat. Commun. **5**, 4333 (2014).
- [80] K. Nakata, J. Klinovaja, and D. Loss, Phys. Rev. B **95**, 125429 (2017).

Floquet Topological Magnons: Supplemental Material

S. A. Owerre¹

¹*Perimeter Institute for Theoretical Physics, 31 Caroline St. N., Waterloo, Ontario N2L 2Y5, Canada.*

I. TOPOLOGICAL MAGNON PHASE DIAGRAM

For a fixed λ such that $\mathcal{J}_n(\lambda) \neq 0$ the honeycomb Floquet topological magnons maps to the static XXZ ferromagnetic quantum spin Hamiltonian with DM interaction

$$\mathcal{H} = - \sum_{\langle\alpha,\beta\rangle} [J_{\perp}(S_{\alpha}^x S_{\beta}^x + S_{\alpha}^y S_{\beta}^y) + J_z S_{\alpha}^z S_{\beta}^z] \quad (1)$$

$$+ D \sum_{\langle\langle\alpha,\beta\rangle\rangle} \nu_{\alpha\beta} \hat{\mathbf{z}} \cdot \mathbf{S}_{\alpha} \times \mathbf{S}_{\beta} - J_2 \sum_{\langle\langle\alpha,\beta\rangle\rangle} \mathbf{S}_{\alpha} \cdot \mathbf{S}_{\beta}.$$

We have added an isotropic next-nearest-neighbour (NNN) ferromagnetic exchange coupling J_2 and $J_z > J_{\perp}$ as before. In the bosonic representation we obtain

$$\mathcal{H} = -t_{\perp} \sum_{\langle\alpha\beta\rangle} (a_{\alpha}^{\dagger} a_{\beta} + h.c.) - t_2 \sum_{\langle\langle\alpha\beta\rangle\rangle} (e^{i\phi_{\alpha\beta}} a_{\alpha}^{\dagger} a_{\beta} + h.c.) \quad (2)$$

$$+ t_A \sum_{\alpha \in A} a_{\alpha}^{\dagger} a_{\alpha} + t_B \sum_{\alpha \in B} a_{\alpha}^{\dagger} a_{\alpha}.$$

The mean-field energy has been dropped. $t_{\perp} = J_{\perp} S$, $t_2 = \sqrt{t_2^2 + t_D^2}$, $t_2(t_D) = J_2 S(DS)$, $t_{A(B)} = 3J_{z,A(B)} S + 6J_2 S$. The phase factor is $\phi_{\alpha\beta} = \nu_{\alpha\beta} \phi$, where $\phi = \arctan(t_D/t_2')$ is a magnetic flux generated by the DM interaction on the NNN sites.

Next, we Fourier transform the magnon hopping Hamiltonian (2) into momentum space and the resulting Hamiltonian can be written as $\mathcal{H} = \sum_{\mathbf{k}} \psi_{\mathbf{k}}^{\dagger} \cdot \mathcal{H}(\mathbf{k}) \cdot \psi_{\mathbf{k}}$, with $\psi_{\mathbf{k}}^{\dagger} = (a_{\mathbf{k}A}^{\dagger}, a_{\mathbf{k}B}^{\dagger})$. The momentum space Hamiltonian is given by

$$\mathcal{H}(\mathbf{k}) = d_0(\mathbf{k}) \mathbf{I} + \mathbf{d}(\mathbf{k}) \cdot \boldsymbol{\sigma}, \quad (3)$$

where \mathbf{I} is an identity 2×2 matrix and $\boldsymbol{\sigma} = (\sigma_x, \sigma_y, \sigma_z)$ are Pauli matrices and $\mathbf{d} = (d_x, d_y, d_z)$ are given by

$$d_0(\mathbf{k}) = \epsilon_0 - 2t_2 \cos \phi \sum_j \cos \mathbf{k} \cdot \mathbf{b}_j, \quad (4)$$

$$d_x(\mathbf{k}) = -t_{\perp} \sum_j \cos \mathbf{k} \cdot \boldsymbol{\delta}_j, \quad (5)$$

$$d_y(\mathbf{k}) = -t_{\perp} \sum_j \sin \mathbf{k} \cdot \boldsymbol{\delta}_j, \quad (6)$$

$$d_z(\mathbf{k}) = M - 2t_2 \sin \phi \sum_j \sin \mathbf{k} \cdot \mathbf{b}_j, \quad (7)$$

with $\epsilon_0 = (t_A + t_B)/2 + 6J_2 S$ and $M = (t_A - t_B)/2$. The magnon bands are given by

$$\varepsilon_s(\mathbf{k}) = d_0 \pm \sqrt{\mathbf{d} \cdot \mathbf{d}} = d_0 + s\varepsilon(\mathbf{k}), \quad (8)$$

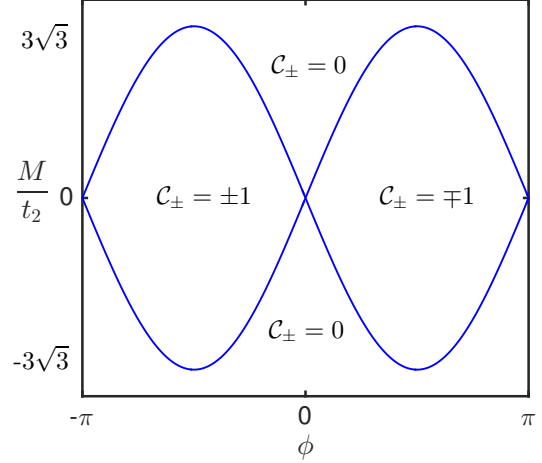


FIG. 1. The complete phase diagram of the Haldane magnon insulator. In the topological magnon insulator regime $C_{\pm} = \pm 1$ and in the trivial magnon insulator $C_{\pm} = 0$.

where $s = \pm$ for the upper and lower magnon bands respectively. The eigenvectors are given by

$$|\psi_{s\mathbf{k}}\rangle = \frac{1}{\sqrt{2}} \begin{pmatrix} \sqrt{1 + s \frac{d_z(\mathbf{k})}{\epsilon(\mathbf{k})}}, & -s e^{-i\varphi_{\mathbf{k}}} \sqrt{1 - s \frac{d_z(\mathbf{k})}{\epsilon(\mathbf{k})}} \end{pmatrix}^T, \quad (9)$$

where

$$\tan \varphi_{\mathbf{k}} = \frac{d_y(\mathbf{k})}{d_x(\mathbf{k})}. \quad (10)$$

A. Magnon phase transition

The model above is termed a Haldane magnon insulator. It has only been studied in the topological phase, which is the only phase one would get at the isotropic point $J_{\perp} = J_z$ [1, 2] (see also [3]). Therefore, the full topological phase diagram of the Haldane magnon insulator has not been mapped out. In this section, we will present the complete topological phase diagram of Haldane magnon insulator and also show that it differs from the electronic counterpart [4] in terms of transport properties. For $\phi \neq n\pi$, the magnon bands have nonzero Berry curvature $\Omega_{s\mathbf{k}} = (\nabla \times \mathcal{A}_{s\mathbf{k}})_z$ where $\mathcal{A}_{s\mathbf{k}} = i \langle \psi_{s\mathbf{k}} | \nabla | \psi_{s\mathbf{k}} \rangle$ is the Berry connection. The Chern number is given by

$$\mathcal{C}_s = \frac{1}{2\pi} \int d^2k \Omega_{s\mathbf{k}}. \quad (11)$$

The maximum contribution to the Berry curvature comes from the states near the corners of the Brillouin zone $\mathbf{K}_\tau = (\tau 4\pi/3\sqrt{3}, 0)$ with $\tau = \pm$. Therefore, we expand the Hamiltonian near this point and the differential operator can be expressed in polar coordinates (k, ϕ_k) where $k = |\mathbf{k}|$. The Berry curvature takes the form

$$\Omega_{ks}^\tau = \frac{1}{k} \left(\frac{\partial(k\mathcal{A}_{s\varphi_k}^\tau)}{\partial k} - \frac{\partial\mathcal{A}_{sk}^\tau}{\partial\varphi_k} \right), \quad (12)$$

where $\mathcal{A}_{s\varphi_k}^\tau = \frac{1}{k} i \langle \psi_{ks}^\tau | \partial_{\varphi_k} \psi_{sk}^\tau \rangle$ and $\mathcal{A}_{sk}^\tau = i \langle \psi_{ks}^\tau | \partial_k \psi_{sk}^\tau \rangle$. We note that φ_k appears as a U(1) phase in the eigenvectors, therefore $\mathcal{A}_{s\varphi_k}^\tau$ and \mathcal{A}_{sk}^τ are independent of φ_k , thus the second term in Eq. 12 vanishes and the resulting expression becomes

$$\Omega_{ks}^\tau = \frac{1}{k} \frac{\partial}{\partial k} \mathcal{P}_s^\tau(k); \quad \mathcal{P}_s^\tau(k) = i \langle \psi_{sk}^\tau | \partial_{\phi_k} \psi_{sk}^\tau \rangle. \quad (13)$$

By integrating the Berry curvature we obtain

$$\mathcal{C}_s = \sum_{\tau=\pm} [\mathcal{P}_s^\tau(\infty) - \mathcal{P}_s^\tau(0)], \quad (14)$$

$$= -\frac{s}{2} \sum_{\tau=\pm} \tau \text{sgn}[M + 3\sqrt{3}\tau t_2 \sin\phi]. \quad (15)$$

A topological magnon phase transition occurs at $M_c = 3\sqrt{3}t_2 \sin\phi$. The regime $M < M_c$ corresponds to a topological magnon Chern insulator with $\mathcal{C}_\pm = \mp 1$ and the regime $M > M_c$ corresponds to a trivial magnon insulator with $\mathcal{C}_\pm = 0$. The phase diagram of the Haldane magnon insulator is depicted in Fig. 1. From bulk-edge correspondence we expect chiral magnon edge modes in the vicinity of the bulk gap, which are protected by the Chern numbers. As shown in Fig. 2, the topological regime possesses gapless chiral magnon edge modes whereas the chiral magnon edge modes in the trivial magnon insulator regime contribute to the bulk magnon bands.

B. Magnon quantum anomalous Hall effect

In electronic systems, quantum anomalous Hall effect refers to the generation of a transverse quantized Hall conductivity without an applied magnetic field. Basically, an electric field \mathcal{E} induces a charge current \mathcal{J}_e and the Berry curvature acts as an effective magnetic field in momentum space. For insulating quantum ferromagnets the magnon excitations are charge-neutral and do not experience a Lorentz force. Instead, a temperature gradient $-\nabla T$ induces a heat current \mathcal{J}_Q , and the Berry curvature due to the DMI appears in the equations of motion of a magnon wave packet in the same mathematical structure as a magnetic field in the Lorentz force.

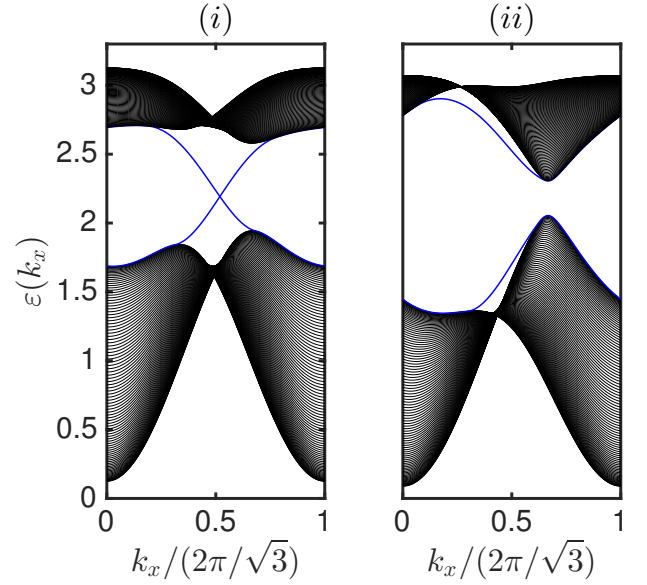


FIG. 2. Topological and trivial magnon insulator phases on the honeycomb quantum ferromagnets for $(t'_2 = t_D = t_2 = 0.2t_\perp)$ or $\phi = \pi/4$. The parameters are chosen such that the phase transition occurs at $(M/t_\perp)_c \approx 0.73$ where the magnon bulk gap closes (not shown). (i) Topological Chern magnon insulator with gapless magnon edge modes (blue lines) for $M/t_\perp = .1$. (ii) Trivial magnon insulator with bulk gap and no gapless magnon edge modes (blue lines) for $M/t_\perp = 1$.

In ferromagnets, this does not require an applied magnetic field analogous to the electronic counterparts. The thermal Hall conductivity is given by

$$\kappa_{xy} = -\frac{k_B^2 T}{(2\pi)^2} \sum_{s=\pm} \int_{BZ} d^2k c_2(n_s) \Omega_{s\mathbf{k}}, \quad (16)$$

where $n_s \equiv n_B[\varepsilon_{s\mathbf{k}}] = [e^{\varepsilon_{s\mathbf{k}}/k_B T} - 1]^{-1}$ is the Bose function, $c_2(x) = (1+x) (\ln \frac{1+x}{x})^2 - (\ln x)^2 - 2\text{Li}_2(-x)$, and $\text{Li}_n(x)$ is a polylogarithm.

The major difference here is that magnon transports require a finite temperature due to the Bose function. In other words, magnonic systems do not have conduction and valence bands and no bands are fully occupied or completely empty. Instead, the magnons can be thermally populated at low temperatures near the $\mathbf{k} = 0$ mode. In fact, the maximum contribution of κ_{xy} comes from the lowest magnon band near the $\mathbf{k} = 0$ mode at low temperatures.

Unlike electronic systems, the topological and the trivial insulating regimes in Fig. 2 will possess a finite κ_{xy} due to the population of the band near the $\mathbf{k} = 0$ mode at low temperatures. In this limit the Berry curvature of the lowest band in the topological and trivial insulating phases has the form

$$\Omega_-(\mathbf{k} \rightarrow 0) \simeq \frac{c_1 k_x k_y^2 + c_2 k_x^2 k_y^2}{c_3}, \quad (17)$$

where $c_1 = -27(Mt_2)/8$, $c_2 = 81\sqrt{3}t_2 \sin \phi/8$ and $c_3 = 4(M^2 + 9t_2^2)^{3/2}$. In the low-temperature limit κ_{xy} can be well-approximated as

$$\kappa_{xy} \simeq \frac{1}{T} \int \frac{d^2k}{(2\pi)^2} n_B[\varepsilon_-(\mathbf{k})][\varepsilon_-(\mathbf{k}) + \varepsilon_+(\mathbf{k})]^2 \Omega_-(\mathbf{k}). \quad (18)$$

Near the $\mathbf{k} = 0$ mode, $\varepsilon_-(\mathbf{k}) + \varepsilon_+(\mathbf{k}) \simeq 2(t_A + t_B) = t_0$ and $\varepsilon_-(\mathbf{k}) \simeq a + bk^2$, where $a = (t_A + t_B)/2 - 3t_\perp$ and $b = 3t_\perp/4$. Now, we can parameterize the momentum

in the polar coordinate ($k_x = k \cos \theta$, $k_y = k \sin \theta$) and perform the angular part of the integration,

$$\begin{aligned} \kappa_{xy} &\simeq \frac{c_2}{c_3} \frac{t_0^2}{16\pi T} \int_0^\infty k dk \frac{k^4}{e^{(a+bk^2)/T} - 1}, \\ &= \frac{T^2}{16\pi b^3} \frac{c_2}{c_3} \text{Li}_3 \left[\exp \left(-\frac{a}{T} \right) \right]. \end{aligned} \quad (19)$$

This is the low-temperature thermal Hall conductivity in the topological and trivial insulating phases.

-
- [1] S. A. Owerre, J. Phys.: Condens. Matter **28**, 386001 (2016).
 [2] S. A. Owerre, J. Appl. Phys. **120**, 043903 (2016).
 [3] S. K. Kim et.al., Y. Tserkovnyak, Phys. Rev. Lett. **117**,

- 227201 (2016).
 [4] F. D. M. Haldane, Phys. Rev. Lett. **61**, 2015 (1988).